Macromolecules

Article

pubs.acs.org/Macromolecules

Nonequilibrium Simulations of Lamellae Forming Block Copolymers under Steady Shear: A Comparison of Dissipative Particle Dynamics and Brownian Dynamics

Brandon L. Peters,[†] Abelardo Ramírez-Hernández,[†] Darin Q. Pike,[‡] Marcus Müller,[§] and Juan J. de Pablo*[,†,⊥]

[†]Department of Chemical and Biological Engineering, University of Wisconsin—Madison, Madison, Wisconsin 53706, United States

[‡]Sandia National Laboratories, Albuquerque, New Mexico 87185, United States

[§]Institut für Theoretische Physik, Georg-August Universität, 37077 Göttingen, Germany

[⊥]Institute for Molecular Engineering, University of Chicago, Chicago, Illinois 60637, United States

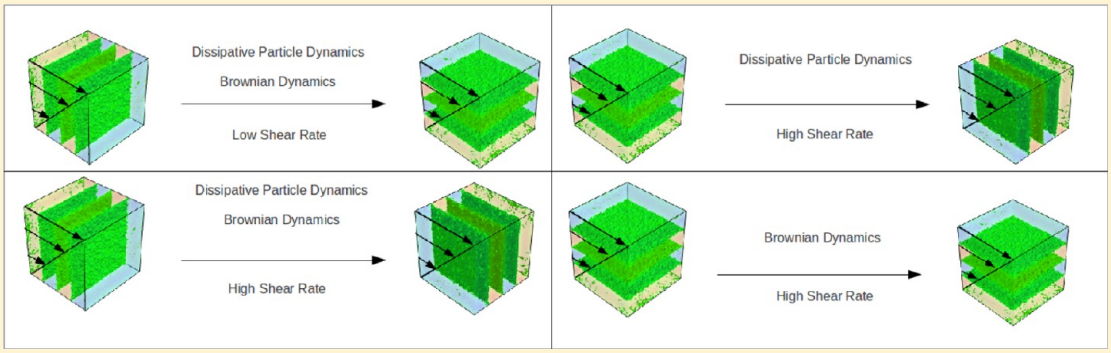

ABSTRACT: Nonequilibrium simulations of lamellae-forming block copolymers are investigated by means of theoretically informed coarse-grained Brownian dynamics simulations and dissipative particle dynamics. Three lamellar orientations are subjected to steady shear, which differ in the direction of the microstructure with respect to the shear plane. The stable orientations are identified as a function of shear rate. It is found that for Brownian dynamics simulations the transition from parallel to perpendicular does not occur; however, by including local conservation of momentum, the lamellae exhibit this transition. The velocity profiles, stresses, and angles of the blocks in the system were analyzed to yield insights into why parallel orientations are less stable at higher shear rates.

INTRODUCTION

Diblock copolymers are macromolecules that consist of two distinct polymer blocks connected by a covalent bond. These materials may microphase separate into nanoscale structures with characteristic dimensions on the order of 10−100 nm.[1] Such dimensions are dictated by the degree of polymerization, the volume fraction of the blocks, and the immiscibility of the blocks.[2] Interest has been growing in the application of block copolymers to nanoscale fabrication, where the self-assembly of block copolymers can be directed by surface patterns, thereby creating templates for synthesis of organic and inorganic structures such as nanowires,[3−5] quantum dots,[6,7] magnetic storage media,[8] and silicon capacitors.[9] In the context of lithographic fabrication, attention has focused on the ability to control the self-assembly and orientation of the nanodomains.[10]

At equilibrium, diblock copolymers exhibit three major morphologies, namely lamellae, hexagonally packed cylinders, and spheres in a body-centered-cubic lattice. These self-assembled structures may be globally ordered by shear flow,[11−17] chemical patterns,[10,18−20] graphoepitaxy, and solvent annealing.[21,22] The lamellar structures and their response to steady shear flow are the focus of this paper. Figure 1 shows three distinct lamellar orientations that are subjected to shear; these are labeled parallel (∥), perpendicular (⊥), and transverse ($\mathcal{T}$), according to the normal of the lamellae with respect to the direction of the shear plane. The lamellae normals are

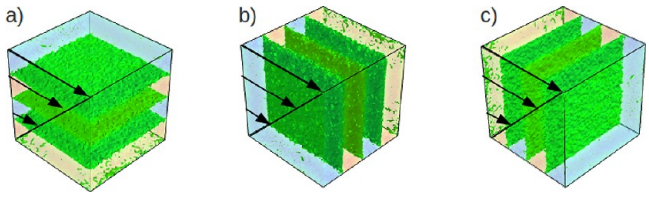

Figure 1. Schematic representation of lamellae: (a) parallel (∥), (b) perpendicular (⊥), and (c) transverse ($\mathcal{T}$) orientations. Figures were generated using an Open-Source Scientific Visualization Software, Mayavi2.[23]

Received: July 23, 2012
Published: October 1, 2012

parallel to the velocity gradient, the vorticity, and the flow direction, respectively.

Depending on frequency and strain, the application of an oscillatory flow to copolymer melts or solutions just below the order−disorder transition (ODT) results in stable ∥ and ⊥ orientations. Initially, Koppi et al.[24,25] found that the perpendicular morphology was obtained at high frequencies and elevated temperatures, and the parallel morphology was observed otherwise; their experiments were conducted on a poly(ethylene propylene)-*b*-poly(ethylethylene) (PEE-*b*-PEP) block copolymer. The transition from the parallel morphology to the perpendicular morphology was also seen at higher frequencies, but the reverse was not found. For polystyrene-*b*-polyisoprene (PS-*b*-PI), Patel et al.[26] and Riise et al.[27] obtained the parallel orientation at high frequencies and the perpendicular orientation at low frequencies. Gupta et al.[28] showed that at high frequencies the parallel morphology is stable and at lower frequencies the perpendicular morphology is stable for a PS-*b*-PI lamellae-forming block copolymer. Leist et al.[29] found two transitions from ∥ → ⊥ → ∥ as the oscillatory frequency was lowered. Leist et al.[29] showed that the shear rate can be mapped directly onto the oscillatory shear. The flip back to parallel at higher shear rates is in contradiction with the theoretical work of Fredrickson;[30] lack of a double flip in theory has been attributed to wall flow interactions in the experiments.[31] The reviews by Chen and Kornfield[32] and Hamley[33] provide an extensive discussion of the morphologies observed in experiments. In general, the deformation of the block copolymer comes from large-amplitude oscillatory shear (LAOS), where the oscillatory frequency governs the reorientation of the lamellar structures.[12,24−27]

Several theoretical studies have considered the effect of steady shear on lamellar-forming block copolymers in the bulk.[30,31,34−36] Fredrickson[30] performed a study using a mean-field block copolymer model with a simple stochastic model of the dynamics and showed that near the ODT, at low shear stress, the parallel morphology is stable, and at higher shear stress the perpendicular morphology is stable. This study did not examine the actual transition between the parallel orientation and the perpendicular orientation. Rychkov[31] used nonequilibrium molecular dynamics using a Lennard-Jones (LJ) polymer model and SLLOD equations of motion for planar Couette shear flow and found that sphere and cylinder forming block copolymers in solution change morphology, to the parallel lamellar orientation at low shear rates, and to the perpendicular lamellar orientation at higher shear rates. Cui et al.[37] used self-consistent field theory with the lattice Boltzmann method to find the stable orientations of a symmetric block copolymer. At low shear frequencies a parallel orientation was observed, and at higher frequencies a perpendicular morphology was seen. Note that their initial state was disordered.

Guo et al.[34] studied lamellae-forming block copolymers using short chains of LJ particles with a dissipative particle dynamics (DPD) thermostat using the reverse nonequilibrium algorithm of Müller−Plathe (MP) to induce a shear velocity profile. The transitions from $\mathcal{T} \rightarrow \parallel$ and $\mathcal{T} \rightarrow \perp$ were observed; at low shear rates, the parallel morphology was stable, and at higher shear rates the perpendicular morphology was stable. Later, Guo[35] used a similar model to study the transition from ∥ → ⊥; the kinetic mechanism was found to be through an undulation instability, partial breakup of monodomains, domain rotation, and recombination coupled to defect migration and annihilation. Liu et al.[36] used the standard DPD model of short block copolymers developed by Groot et al.[38−40] They described a mechanism in which lamellar layers are distorted and then evolve to the perpendicular orientation. The article also shows chevron instabilities in the strong segregation limit and sinusoidal instabilities in the weak segregation regime for different values of the Flory−Huggins parameter (χN). Fraser et al.[41] used the same block copolymer DPD model to look at the stability of ∥ and ⊥. It was found that ∥ has higher internal energy and a larger entropy production than ⊥ and concluded that ⊥ should be more stable at higher shear rates. Lísal and Brennan[42] performed a similar study to that of Fraser et al. and found that there is also a metastable diagonal lamellar morphology. These articles employed a DPD thermostat because it is believed that hydrodynamic interactions play a role in the mechanisms behind morphological transitions under nonequilibrium conditions.[34,35] A review of simulation techniques for shearing polymer melts or solutions has been presented by Rychkov.[31]

The motivation for the present study is twofold: first, we aim to extend a coarse-grained formalism for description of block copolymer assembly that has been particularly helpful under equilibrium to nonequilibrium situations. Eventually, we would like to investigate the dynamics of copolymer assembly on chemical nanopatterns.[43−45] Note that past reports on equilibrium Monte Carlo simulations using the model considered here have shown good agreement with experiments;[10,46−53] there is reason to expect that such agreement will continue in out-of-equilibrium situations. Second, we seek to investigate the behavior of copolymer lamellae under shear and determine the source of the discrepancies between the predictions of different theoretical approaches.

Specifically, in this work we implement a particle-based theoretically informed block copolymer model[10,46−53] in Brownian dynamics simulations with both a conventional thermostat and a dissipative particle dynamics thermostat and we examined its behavior under shear flow using Lees−Edwards boundary conditions.[54] We examine the differences that arise when conservation of local momentum is enforced through DPD thermostats or simple white noise.

METHODS AND MODEL

The coarse-grained model employed in this work has been described in the literature;[10,46−53] it takes into account the main characteristics of copolymers, including chain connectivity, compressibility, and the incompatibility of the monomers. Each chain is discretized into N beads; the position of the sth bead on the ith chain is denoted by $\mathbf{r}_i(s)$. The total Hamiltonian can be written as the sum of bonded contributions (H_b) and nonbonded contributions (H_{nb}):

$$H(\mathbf{r}_i(s)) = H_b(\mathbf{r}_i(s)) + H_{nb}[\phi_A, \phi_B] \tag{1}$$

where $H_b(\mathbf{r}_i(s))$ is given by

$$\frac{H_b(\mathbf{r}_i(s))}{k_B T} = \frac{3}{2} \sum_{i<j} \left(\frac{r_{ij}}{b}\right)^2 B_{ij} \tag{2}$$

and H_{nb} is given by

$$\frac{H_{nb}[\phi_A, \phi_B]}{k_B T} = \sqrt{\bar{N}} \int_V \frac{\mathrm{d}r}{{R_e}^3} \left[\chi N \phi_A \phi_B + \frac{\kappa N}{2} (\phi_A + \phi_B)^2\right] \tag{3}$$

The sum in eq 2 runs over all beads (Nn) (where n is the number of chains and N is the number of beads per chain), B_{ij} is either unity if there is a bond linking the beads or zero otherwise, $\phi_K(\mathbf{r})$ is the normalized local density of type K beads, ρ_0 is the number density of the beads, V is the volume, and $\sqrt{\bar{N}}$ is the number of chains per unit chain volume, which can be extracted from experiments. The interdigitation number is defined by $\sqrt{\bar{N}} = \rho_0 {R_e}^3$,[47] where R_e is the average end-to-end distance and $b^2 = {R_e}^2/(N-1)$. Essentially, $\bar{N}$ controls the strength of the fluctuations; it can be estimated from the molecular weight and melt density determined from experiments.[55] The strength of nonbonded interactions between a homopolymer of type A with a homopolymer of type B is determined by the Flory–Huggins parameter (χ), and κ ensures that there is a continuous density throughout the system (a description for the choice of κ is given in Pike et al.[46]).

By defining a density cloud ($\omega(\mathbf{r})$) around each particle's position, one can compute the beads' local densities ϕ_K. The integral in eq 3 can therefore be written as a sum of pairwise interactions between beads where K is either type A or B.

$$U_{ij} = \frac{\sqrt{\bar{N}}}{{R_e}^3}[\kappa N + \chi N(1-\delta_{KK})] \int_V \omega(\mathbf{r}-\mathbf{r}_i)\omega(\mathbf{r}-\mathbf{r}_j)\,\mathrm{d}r \tag{4}$$

The density cloud decays to zero at a cutoff distance r_{int}, which allows for each bead to have a sufficient number of interactions with neighbors, as determined in Detcheverry et al. and Pike et al.[47,46] Spherical step-like functions are used to determine the interactions, so the beads can be thought of as soft spheres where the pairwise interaction energy is proportional to the overlapping volume of the density clouds. The density clouds are normalized to unity, so $\omega(\mathbf{r}) = C\tilde{\omega}(r)$, where $\tilde{\omega}(r) = 1$ if $r \le r_{int}$, $\tilde{\omega}(r) = 0$ if $r \ge r_{int}$, and C is a normalization constant ($1/4/3\pi\ {r_{int}}^3$). Following Pike et al., in our simulations each bead interacts on average with 14 beads.

The model described above can be implemented using Brownian dynamics with simple white noise; the evolution of the particles is described by

$$\gamma\frac{\mathrm{d}\mathbf{r}_i}{\mathrm{d}t} = \mathbf{f}_i^{\mathrm{b}}(t) + \mathbf{f}_i^{\mathrm{nb}} + \zeta_i(t) \tag{5}$$

where $\mathbf{r}_i$ is the position vector of bead i, γ is the friction coefficient, $\mathbf{f}_i^{\mathrm{b}}$ and $\mathbf{f}_i^{\mathrm{nb}}$ are the bonded and nonbonded forces on particle i, respectively, given by $\mathbf{f} = -\nabla U$, and ζ is a Gaussian random vector of independent Wiener process with zero mean, unit variance, and $\langle\zeta^2\rangle = 2\gamma k_B T$. In the limit of the nonbonded interactions going to zero, the Brownian dynamics equation gives rise to the Rouse model. A discussion of this implementation in equilibrium can be found in Ramírez-Hernández et al.[56]

The Brownian dynamics approach outlined above does not conserve momentum. Groot et al.[38,39] used a DPD thermostat in Brownian dynamics simulations of block copolymers and showed that hydrodynamics plays an important role in the kinetics of microphase separation of hexagonally packed cylinders. Furthermore, previous theoretical work has shown that DPD reproduces the transition $\parallel \rightarrow \perp$. More generally, several reports have highlighted the importance of DPD thermostats in nonequilibrium flows.[34,35,37] The DPD model consists of the summation of conservative forces (F^{C}), noise (F^{R}), and dissipative forces (or friction) (F^{D}). The conservative forces for this paper are derived from the forces from the Hamiltonian in eq 1. The random forces and dissipative forces on each particle, respectively, are given by

$$\mathbf{F}_i^{\mathrm{R}} = \sigma\sum_{i<j}\omega^{\mathrm{R}}(\mathbf{r}_{ij})\hat{\mathbf{r}}_{ij}\zeta_{ij}/\sqrt{\delta t}$$
$$\mathbf{F}_i^{\mathrm{D}} = -\gamma\sum_{i<j}\omega^{\mathrm{D}}(\mathbf{r}_{ij})(v_{ij}\cdot\mathbf{r}_{ij})\hat{\mathbf{r}}_{ij} \tag{6}$$

where ζ_{ij} is a random vector with zero mean and unit variance for a pair of particles (i, j), $\mathbf{v}_{ij} = \mathbf{v}_i - \mathbf{v}_j$, and $\mathbf{r}_{ij}$ is the vector between two beads. The weight function is given by

$$[\omega^{\mathrm{R}}]^2 = \omega^{\mathrm{D}} = \begin{cases} 1 - r/r_{\mathrm{int}}, & r < r_{\mathrm{int}} \\ 0, & r \ge r_{\mathrm{int}} \end{cases} \tag{7}$$

which is common in the DPD literature and $\sigma = (2\gamma k_B T)^{1/2}$.[58,59] To evolve the beads in time, a modified velocity-Verlet algorithm is used according to

$$\mathbf{r}_i(t+\delta t) = \mathbf{r}_i(t) + \delta t\mathbf{v}_i(t) + \frac{1}{2}\delta t^2\mathbf{f}_i(t)$$
$$\tilde{\mathbf{v}}_i(t+\delta t) = \mathbf{v}_i(t) + \frac{1}{2}\delta t\mathbf{f}_i(t)$$
$$\mathbf{f}_i(t+\delta t) = \mathbf{f}_i(\mathbf{r}_i(t+\delta t)),\ \tilde{\mathbf{v}}_i(t+\delta t))$$
$$\mathbf{v}_i(t+\delta t) = \tilde{\mathbf{v}}_i(t+\delta t) + \frac{1}{2}\delta t(\mathbf{f}_i(t) + \mathbf{f}_i(t+\delta t)) \tag{8}$$

where δt is the time step, $\mathbf{v}_i$ is the velocity of bead i, $\tilde{\nu}_i$ is the half-step velocity of the bead, and $\mathbf{f}_i$ is the sum of the conservative forces, random forces, and dissipative forces. A value of $\delta t = 0.01$ is used for the simulations.

Common methods for including shear in simulations include the approach of Müller-Plathe[60] or the use of Lees–Edwards (LE) periodic boundary conditions.[54] Here we used LE periodic boundary conditions, which impart an average velocity gradient or shear rate ($\bar{\dot{\gamma}}$). The local gradient of the velocity profile is $\dot{\gamma} = \mathrm{d}\nu_x/\mathrm{d}r_z$. Figure 2 provides a schematic representation of the algorithm is shown. For the Brownian dynamics case, the positions are updated by adding an external flow-field in the x direction

$$\mathbf{f}_{i,x}^{\mathrm{drag}} = \bar{\dot{\gamma}}\gamma\left(r_{i,z}(t) - \frac{L_z}{2}\right) \tag{9}$$

where $\bar{\dot{\gamma}} = V_D/L_z$ is the average shear rate and $V_D/2$ is the velocity at the top of the simulation box, $\dot{\gamma} = \partial\nu_x/\partial_z$ is the local shear rate, L_z is the height of the simulation box in the z direction, and the total force on particle i is now $\mathbf{f}_i = \mathbf{f}_i^{\mathrm{b}} + \mathbf{f}_i^{\mathrm{nb}} + \mathbf{f}_{i,x}^{\mathrm{drag}}$. In what follows, this method will be referred to as Brownian dynamics flow (BDF).

For the DPD thermostat, LE periodic boundary conditions are used to shear the block copolymers as follows. When a bead crosses the boundary in the z direction, the velocities are updated in the x direction, but the y and z velocities remain the same:

$$v_{i,x}(t) = v_{i,x}(t) \pm V_D \tag{10}$$

where the positive sign is used when the beads cross in the negative z direction and the negative sign is used when the beads cross in the positive z direction. This method is simply

dx.doi.org/10.1021/ma301541f | Macromolecules 2012, 45, 8109–8116

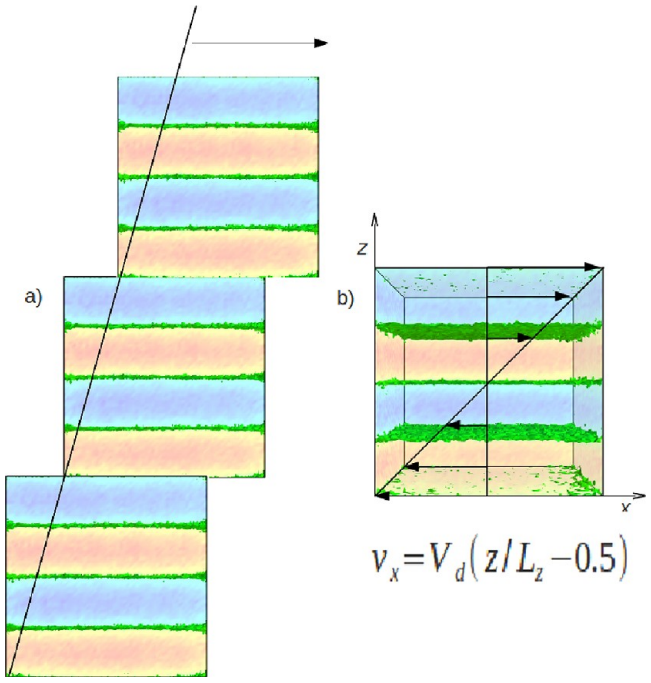

Figure 2. Schematic representation of the Lees–Edwards periodic boundary conditions. (a) is a representation of how the system is implemented, and (b) is the final velocity profile. Figures were generated using an Open-Source Scientific Visualization Software, Mayavi2.[23]

referred to as DPDT. An important difference between the methods used here is that in BDF a linear velocity profile is enforced, whereas in DPDT the velocity profile is induced by the LE periodic boundary conditions, and may not be linear.

Parameters. A 10K-*b*-10K polystyrene-*b*-polyisoprene near the ODT as in Bates et al. and Leist et al.[61,29] block copolymer was modeled. This corresponds to $\sqrt{N} = 58$, $\chi N = 15$, and $\kappa N = 15$. We choose $N = 32$. The relaxation times ($\tau = R_e^2/D$) are $\tau_{BDF} = 77.485R_e^2/D_0$ and $\tau_{DPDT} = 87.98R_e^2/D_0$, where $D_0 = k_BT/\gamma = 1$ where γ is the friction coefficient and $\sigma = 3.0$. It should be noted that, in contrast to models with steep excluded volume interactions, the friction comes from the thermostat (i.e., the soft nonbonded interactions do not generate significant friction). The prediction of the Rouse model's relaxation time is $\tau_{Rouse} = 88R_e^2/D_0$ in a disordered state.

RESULTS AND DISCUSSION

When evolving the system with BDF, we started with three different lamellar configurations, namely parallel (∥), perpendicular (⊥), and transverse ($\mathcal{T}$), as seen in Figure 1. We performed simulations by increasing the shear rate for each of the three initial configurations. If the initial configuration was $\mathcal{T}$, and the shear rate was turned on, the final stable configuration was ∥. At intermediate shear rates diagonal lamellae were found to be stable. At high shear rates, ⊥ was found to be stable, as seen in Figure 3b,c. This is in agreement with experiments where the stable orientations under the influence of increasing shear rate are ∥ and then ⊥. However, for an initial configuration ∥ or ⊥, increasing the shear rate did not change the lamellar orientations. This is in contradiction with theoretical and experimental results that show a transition ∥ →⊥ at high shear rates. For the initial configuration of $\mathcal{T}$, lamellae undergo a quick disordering transition and then a long

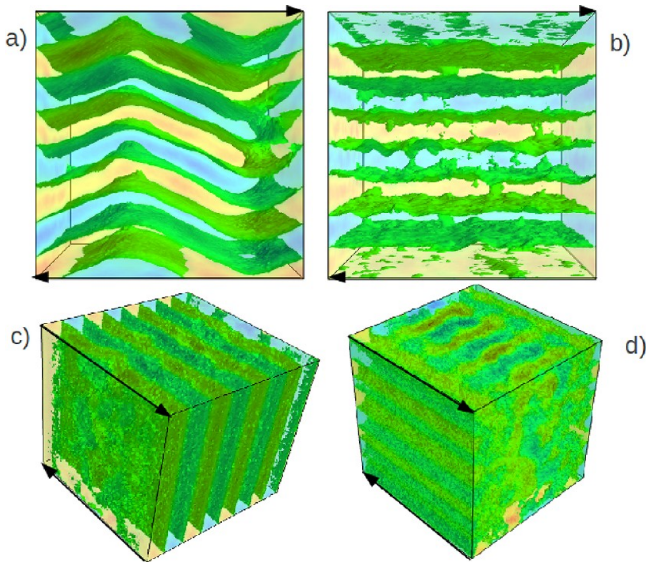

Figure 3. Final simulation snapshots of the initial configuration of $\mathcal{T}$: (a) a sinusoidal ∥ using DPDT at $Wi = \bar{\dot{\gamma}}\tau = 0.70$, (b) ∥ using BDF at $Wi = 6.119$, and (c) ⊥ using DPDT and BDF (qualitatively similar results). (d) A snapshot of $\mathcal{T}$ at $Wi = 6.119$ after 1000 timesteps after shearing. Arrows represent shearing in the x direction. Figures were generated using an Open-Source Scientific Visualization Software, Mayavi2.[23]

reordering phase for both perpendicular and parallel orientations, where the disordered state can be seen in Figure 3d.

Next, the system was evolved with DPDT and the velocity-Verlet algorithm from the same initial configurations. $\mathcal{T}$ is qualitatively similar to that obtained with BDF, where the stable configurations are a sinusoidal ∥ (Figure 3a) and ⊥ (Figure 4e). Since the block copolymers are in the weak segregation limit, they exhibit a sinusoidal final configuration, as in Liu et al.[36] The mechanisms of formation, however, are slightly different. The reordering of the lamellar microstructures happens along the mechanism proposed in Lísal, illustrated in Figure 4, where

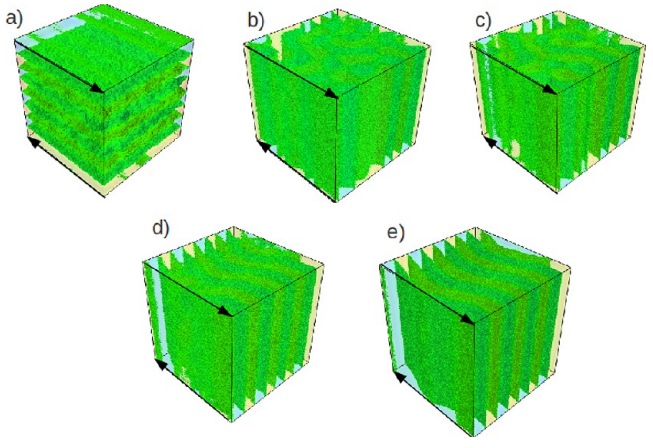

Figure 4. The mechanism for DPDT with ∥ as the initial configuration: (a) 20 000 timesteps, (b) 35 000 timesteps, (c) 40 000 timesteps, and (d) 50 000 timesteps. (e) Final configuration (70 000 timesteps) at $Wi = 31.67$ and for systems with lengths $L_x = L_y = L_z = 4L_0$. Arrows represent shearing in the x direction. Figures were generated using an Open-Source Scientific Visualization Software, Mayavi2.[23]

the lamella break up and then re-form. Major differences come in the changes in ||. At low shear rates the parallel morphology is maintained. However, at intermediate shear rates, a diagonal lamellar orientation is stable. The diagonal state is assumed to be a metastable state.[36,35] The mechanism for the transition || →⊥ is qualitatively similar to that observed in DPD studies with both the reverse nonequilibrium algorithm and Lees–Edwards algorithms.[34−36,41,42] Fluctuations in || eventually force the lamellae to break up, and through a long reorientation process, the lamellae form the final structures seen in Figure 4.

An interesting result is found in the velocity profiles along the gradient for BDF and DPDT. For ⊥, the velocity profile is linear, as in Guo and co-workers.[34] In our implementation, the velocity profile for || has "dips" in it, localized at the interface between block A and block B. Tthis means that the ends of the polymer chains move faster than the middle of the chain when compared to the linear velocity profile. This can be further explained by looking at different values of χN and the stress throughout the simulation box.

Two simulations were run at lower temperatures and a larger molecular weight to ensure that lamellae remain ||. The initial configurations of these simulations were lamellae in the parallel direction, with $Wi = \bar{\dot{\gamma}}\tau = 56.18$. The velocity profile exhibits larger dips at larger values of χN, as seen in Figure 5. In Figure

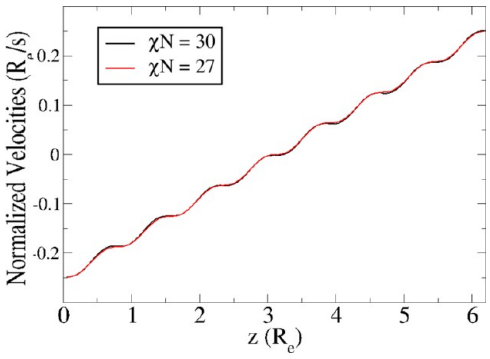

Figure 5. Velocity profiles throughout the simulation box for lengths $L_x = L_y = L_z = 4L_0$ in DPDT simulations.

6, a smaller box is used at the same shear rate with normalized length in the z direction, to accentuate the "dips" for different values of χN. When heating the system, the || begin the transition to the diagonal lamellae, which is expected for this shear rate. If we examine the xx, yy, zz, and xz components of the stress (σ_{xx}, σ_{yy}, σ_{zz}, σ_{xz}), we can infer one reason behind the

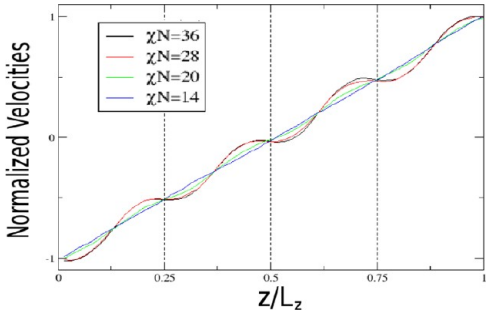

Figure 6. Velocity profiles throughout the simulation box for lengths $L_x = L_y = L_z = 2L_0$ and normalized in the z direction to accentuate the dips. The dotted lines refer to the interfaces for DPDT.

flip from || → ⊥. The local stresses are calculated from the expression

$$\frac{\sigma_{\alpha\beta}}{k_B T} = \sum_i \delta(\mathbf{r} - \mathbf{r}_i)\delta_{\alpha\beta} + \sum_{j>i} r_{ij,\alpha} f_{ij,\beta} \int_0^1 \mathrm{d}s\, \delta(\mathbf{r} - \mathbf{r}_i - s\mathbf{r}_{ij}) \tag{11}$$

where $f_{ij,\beta}$ is the force between bead i and j from the thermostat, bonded, and nonbonded potential; $\alpha, \beta \in \{x, y, z\}$; the global stress is $\sigma_{\alpha\beta} = \int_V \mathrm{d}\mathbf{r}\, \sigma_{\alpha\beta}(\mathbf{r})/V$, and the pressure is $\mathrm{Tr}(\sigma)/3$.

In Figure 7a, we show plots of the xx, yy, and zz components of the stress near the interface with DPD. As expected, in the

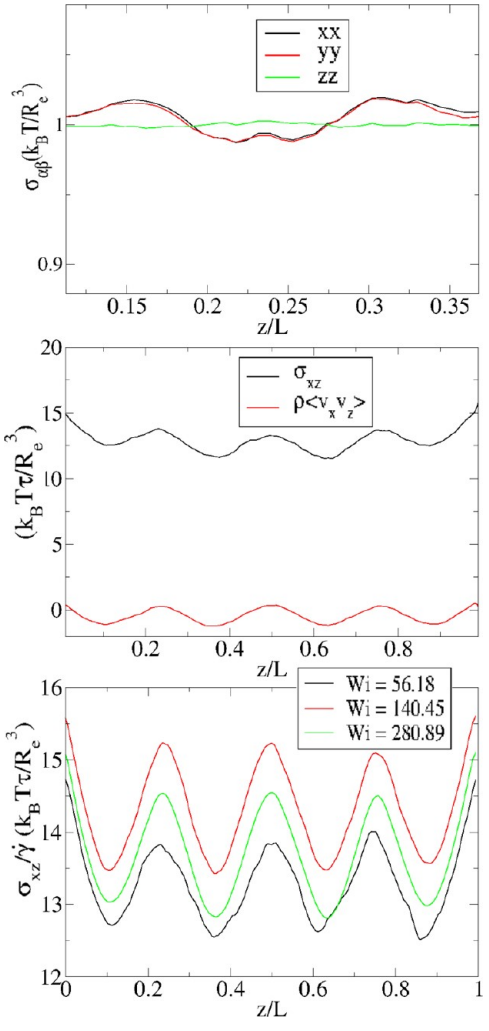

Figure 7. Stress plots for (a) σ_{xx}, σ_{yy}, σ_{zz} at the interface $0.225z/L_z$ without shear, (b) σ_{xz} and $\rho\langle v_x v_z\rangle$ for $Wi = 56.18$, and (c) σ_{xz} for increasing shear rates from $Wi = 56.18$ to $Wi = 280.89$. The interfaces are at 0, 0.225, 0.445, and 0.75 for this system.

absence of shear, the local stress normal to the interfaces in a lamella forming melt is constant, and the tangential stresses exhibit both a minimum and a maximum.[46,62,63] When increasing the shear rate to $Wi = 56.18$ (Figure 7b), distinct minima in σ_{xz} arise at the interface. Although one would initially expect the σ_{xz} profile to be constant throughout the simulation box, in the Appendix we present simple continuum mechanics arguments to justify the observation of the oscillations. There is tumbling motion in the block copolymers

dx.doi.org/10.1021/ma301541f | Macromolecules 2012, 45, 8109–8116

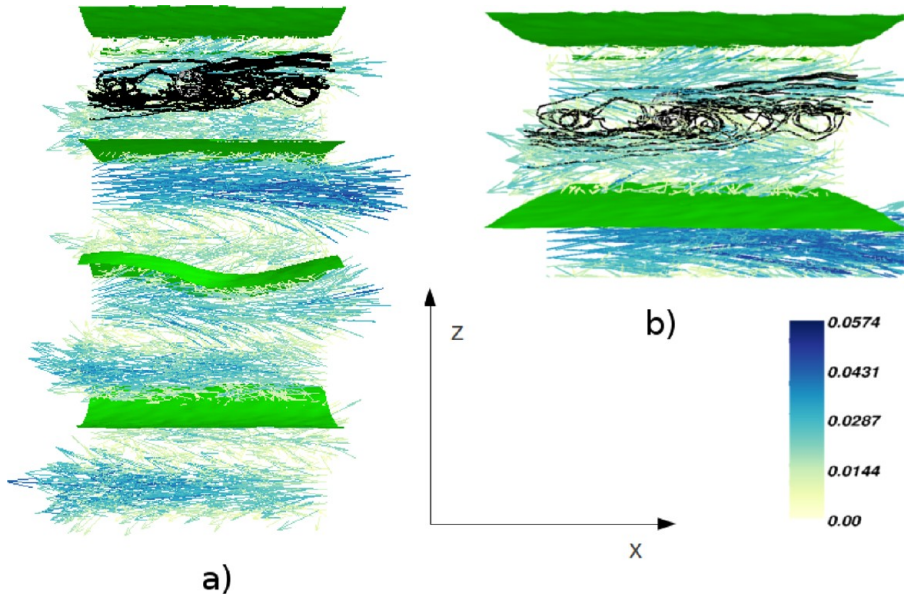

Figure 8. Velocity vector field for Wi = 56.18. The legend from cream to blue corresponds to the magnitude of the velocity vectors (the average velocity gradient has been subtracted $\nu_i = \nu_i - \bar{\dot{\gamma}}\gamma(r_{i,z}(t) - L_z/2)$, green planes show the interfaces between A and B blocks, and black lines represent several stream lines (calculated according to ref 23). (a) Full simulation box of ⊥ lamellae as in Figure 7 and (b) expanded view of the top of the simulation box.

due to a correlation of the x and z velocity components; such motion is apparent in the velocity vector fields shown in Figure 8. When $Wi \rightarrow 0$, the oscillations in $\sigma_{xz}/\bar{\dot{\gamma}}$ vanish (this is discussed in the Appendix). The magnitude of the oscillations decreases as we decrease the Wi number. If we compare the stress plots of the parallel lamellae to the perpendicular lamellae, we can see that the stresses are constant throughout the simulation box (data not shown). This is in agreement with Chen and Kornfield,[32] who pointed out that the polymers are being stretched and have an external stress; to relax, the block copolymers flip to the perpendicular orientation.

Finally, the angles between the block copolymer blocks were analyzed. The vector for each block was calculated from the covalent bond between blocks A and B to the center of mass of each block. As expected, 80% of the angles were between 150° and 180°. This is consistent with results for sheared homopolymers in solution, where the polymers align with the velocity profile.[64,65]

CONCLUSIONS

The transitions from $\mathcal{T} \rightarrow \parallel$ and $\mathcal{T} \rightarrow \perp$ were captured with both BDF and DPDT. The transition from $\parallel \rightarrow \perp$ in the BDF case does not occur, which is in contradiction to literature reports, both experimental and theoretical. With the enforcement of conservation of momentum through the DPD thermostat, the transition from $\parallel \rightarrow \perp$ does occur.

The key differences between our calculations and previous DPD simulations[36,41,42] reside in the densities of the system, the interaction between like and unlike beads, the length of the molecules, and the level of discretization. With respect to the densities, the $\sqrt{\bar{N}}$ used in previous DPD studies is equivalent to 0.3, while the $\sqrt{\bar{N}}$ used in these simulations is 58; this means the systems in the present paper are about 193 times more dense and are experimentally relevant. The discretization of the chains (N) was at most 10 for past DPD studies, and it is 32 for the simulations reported here. This level of coarse-graining may have prevented previous studies from observing the tumbling motion.[66] Five beads per block may not be sufficient to adequately capture fluctuations of molecular shape. The theoretically informed course-grained model also uses the Hamiltonian from Helfand,[67] in contrast to a repulsive term for nonbonded forces employed in previous DPD studies. Guo,[35,34] for example, used an amphiphilic model consisting of only four beads per chain, which would be coarse-grained on a level too large for our purposes. Also, Guo et al. adopted a LJ model.

The theoretically informed coarse-grained model gives useful insights into the reasons why the flip from $\parallel \rightarrow \perp$ occurs. When shearing $\parallel$ at a low temperature, the stresses along the interface are larger than those in the middle of the lamellae. These results show that the "dips" in the velocity profile for $\parallel$ are not artifacts and explain why the beads are moving faster or slower; i.e., it shows why $\parallel$ is not stable at higher shear rates. It is also hypothesized that the inclusion of local conservation of momentum allows for the transition $\parallel \rightarrow \perp$. Finally, we note that the simulations presented here are for unentangled block copolymers near the order−disorder transition and Rouse chains. In the future, we plan to explore the flip with entangled block copolymers, as in the PEP-*b*-PEE block copolymer experiments of Chen et al.[32]

APPENDIX

To examine the oscillations in σ_{xz}, one should look at the conservation of momentum. The Navier−Stokes equation is as follows:

$$\rho\frac{\partial \mathbf{v}}{\partial t} + \rho\mathbf{v}\cdot\nabla\mathbf{v} = \nabla\cdot\sigma + \mathbf{f} \tag{12}$$

where $\mathbf{p}$ is the momentum, $\mathbf{v}(r)$ is the velocity field, ρ is the constant mass density, $\sigma = -p\mathbf{I} + \pi$ is the stress tensor, and $\mathbf{f}$ are the body forces. In our case $\partial\mathbf{v}/\partial t = 0$ because of steady state and $\mathbf{f} = \mathbf{0}$ because the flow is driven by boundary conditions. The hydrodynamic velocity field $\langle\mathbf{v}\rangle$ is obtained by averaging

over a sufficiently large volume element or a sufficiently long time interval, so thermal fluctuations are averaged out. If we look at a microscopic velocity field, as in our simulations, one can average eq 12.

$$\rho\langle \mathbf{v}\cdot\nabla\mathbf{v}\rangle = \rho\left\langle v_x\frac{\partial v_x}{\partial x} + v_y\frac{\partial v_x}{\partial y} + v_z\frac{\partial v_x}{\partial z}\right\rangle = \frac{\partial}{\partial z}\langle\sigma_{zx}\rangle \tag{13}$$

or

$$\frac{\partial}{\partial z}(\langle\sigma_{zx}\rangle - \rho\langle v_x v_y\rangle) = \rho\left\langle \frac{1}{2}v_x\frac{\partial v_x^2}{\partial x} + v_x\frac{\partial v_y}{\partial y} - v_x\frac{\partial v_z}{\partial z}\right\rangle \tag{14}$$

To linear order in velocity, the shear stress, $\langle\sigma_{zx}\rangle$, is independent of the spatial coordinate, z. If one extrapolates the simulation to vanishing shear rate, $\bar{\dot{\gamma}} \to 0$, and plots $\langle\sigma_{zx}\rangle/\bar{\dot{\gamma}}$, where $\bar{\dot{\gamma}}$ is the spatially averaged shear rate, this quantity should become constant. One can also define a local viscosity, $\eta(z)$, from

$$\frac{\langle\sigma_{zx}\rangle}{\bar{\dot{\gamma}}} = \eta(z)\frac{1}{\bar{\dot{\gamma}}}\frac{\partial v_x}{\partial z} \tag{15}$$

This implies that the shear stress is independent from z in the limit $\bar{\dot{\gamma}} \to 0$ and that the spatial dependencies of the local viscosity and the velocity gradient cancel. However, for higher shear rates, there are corrections according to eq 14, which are correlations between different velocity directions. At equilibrium, $\langle v_i v_j\rangle = (k_BT/m)\delta_{ij}$; therefore, corrections have to be induced by the shear, and this observation is compatible with the effect being second-order in v.

If we examine the right-hand side of eq 14, the term proportional to $\partial\langle v_x^2\rangle/\partial x$ is independent of the spatial position because $\langle v_x^2\rangle = k_BT/m$ is establishing the equilibrium value from the thermostat. Second, both v_y and any spatial dependence along the y-direction are small for lamellae oriented with the normal in the z-direction and flow in the x-direction. Lastly, we argue that the correlation induced by the shear flow gives rise to a tumbling motion of the blocks. This tumbling motion has been observed in isolated macromolecules in shear flow and in single molecules tethered to a surface. Given the soft interactions which suppress both static local fluid-like correlations, i.e., packing, as well as any entanglement effects, this tumbling motions also occurs in polymer brushes.[66] This rotational motion gives rise to a perturbation of the velocity field that is approximately proportional to $\mathbf{e}_y \times \mathbf{r}$ and, in this case, the term $\partial v_z/\partial z$ vanishes. Canceling these terms and integrating eq 14 gives the following:

$$\langle\sigma_{zx}\rangle \approx \rho\langle v_x v_z\rangle + \text{const} \tag{16}$$

The result of eq 16 is exactly what is seen in Figure 7b.

Lastly, we note that Noguchi and Gompper[68] have shown that for the DPD thermostat to provide local equilibrium conditions in steady shear, $\bar{\dot{\gamma}} r_{cut} \ll (k_BT/m)^{1/2}$, must be satisfied. Using the cutoff distance from our calculations, we find that according to the requirement, the highest Wi number should be 6.42. Our simulations for the transition from $\| \to \perp$ are carried out at Wi = 29.0−31.67. To verify that we do not have large fluctuations in the thermostat, we calculated $k_BT(z)$ for Wi = 56.18 and 280.89. Both of these values are much larger than the Wi number used for the transition from $\| \to \perp$. In Figure 9, there are oscillations in k_BT and there is a correlation with the velocity profiles. Lower values of the velocity at the interface and larger velocities in the middle of the block. Even at these high shear rates, the oscillations are about 1−2% of the average or less. Moreover, the oscillations become larger at higher shear rates. At a Wi = 31.67, the temperature of the system is 1.014; therefore, we believe the thermostat works properly in these simulations for the transition from $\| \to \perp$.

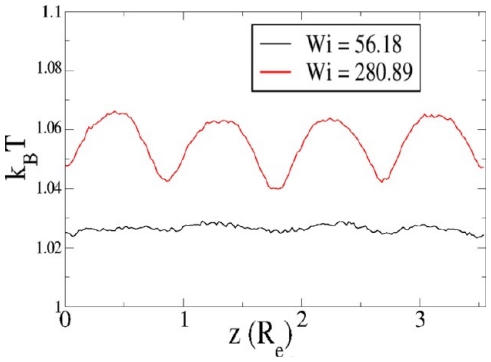

Figure 9. Local distributions of k_BT versus the z-direction. The interfaces are at 0.9, 1.8, and 2.7 R_e.

AUTHOR INFORMATION

Corresponding Author

*E-mail: depablo@uchicago.edu.

Notes

The authors declare no competing financial interest.

ACKNOWLEDGMENTS

This work is supported by the National Science Foundation through the Nanoscale Science and Engineering Center at the University of Wisconsin under Grant DMR-0832760, by the Semiconductor Research Corporation, and the use of the RedSky supercomputer for simulation time. J.J.dP. also thanks the Office of Naval Research for finantial support of the polymer non-equilibrium methodology developed here through the Multi-University Research Initiative (MURI Award N00014-11-1-0690). Marcus Müller acknowledges the SFB 937/A5 for financial support.

REFERENCES

(1) Bates, F.; Fredrickson, G. *Annu. Rev. Phys. Chem.* **1990**, *41*, 525−557.

(2) Bates, F.; Fredrickson, G. *Phys. Today* **1999**, *52*, 32.

(3) Thurn-Albrecht, T.; Schotter, J.; Kastle, G.; Emley, N.; Shibauchi, T.; Krusin-Elbaum, L.; Guarini, K.; Black, C.; Tuominen, M.; Russell, T. *Science* **2000**, *290*, 2126.

(4) Kim, H.; Jia, X.; Stafford, C.; Kim, D.; McCarthy, T.; Tuominen, M.; Hawker, C.; Russell, T. *Adv. Mater.* **2001**, *13*, 795−797.

(5) Lopes, W.; Jaeger, H. *Nature* **2001**, *414*, 735−738.

(6) Park, M.; Harrison, C.; Chaikin, P.; Register, R.; Adamson, D. *Science* **1997**, *276*, 1401.

(7) Li, R.; Dapkus, P.; Thompson, M.; Jeong, W.; Harrison, C.; Chaikin, P.; Register, R.; Adamson, D. *Appl. Phys. Lett.* **2000**, *76*, 1689.

(8) Cheng, J.; Ross, C.; Chan, V.; Thomas, E.; Lammertink, R.; Vancso, G. *Adv. Mater.* **2001**, *13*, 1174−1178.

(9) Black, C.; Guarini, K.; Milkove, K.; Baker, S.; Russell, T.; Tuominen, M. *Appl. Phys. Lett.* **2001**, *79*, 409.

(10) Ruiz, R.; Kang, H.; Detcheverry, F.; Dobisz, E.; Kercher, D.; Albrecht, T.; de Pablo, J.; Nealey, P. *Science* **2008**, *321*, 936.

(11) Angelescu, D.; Waller, J.; Adamson, D.; Deshpande, P.; Chou, S.; Register, R.; Chaikin, P. *Adv. Mater.* **2004**, *16*, 1736−1740.

(12) Okamoto, S.; Saijo, K.; Hashimoto, T. *Macromolecules* **1994**, *27*, 5547−5555.

(13) Zipfel, J.; Lindner, P.; Tsianou, M.; Alexandridis, P.; Richtering, W. *Langmuir* **1999**, *15*, 2599−2602.
(14) Arya, G.; Panagiotopoulos, A. *Phys. Rev. Lett.* **2005**, *95*, 188301.
(15) Chremos, A.; Margaritis, K.; Panagiotopoulos, A. *Soft Matter* **2010**, *6*, 3588−3595.
(16) Arya, G.; Rottler, J.; Panagiotopoulos, A.; Srolovitz, D.; Chaikin, P. *Langmuir* **2005**, *21*, 11518−11527.
(17) Zvelindovsky, A.; Sevink, G.; Fraaije, J. *Phys. Rev. E* **2000**, *62*, 3063−3066.
(18) Stoykovich, M.; Muller, M.; Kim, S.; Solak, H.; Edwards, E.; De Pablo, J.; Nealey, P. *Science* **2005**, *308*, 1442.
(19) Stoykovich, M.; Kang, H.; Daoulas, K.; Liu, G.; Liu, C.; De Pablo, J.; Müller, M.; Nealey, P. *ACS Nano* **2007**, *1*, 168−175.
(20) Kim, S.; Solak, H.; Stoykovich, M.; Ferrier, N.; de Pablo, J.; Nealey, P. *Nature* **2003**, *424*, 411−414.
(21) Marencic, A.; Register, R. *Annu. Rev. Chem. Biomol. Eng.* **2010**, *1*, 277−297.
(22) Segalman, R. *Mater. Sci. Eng., R* **2005**, *48*, 191−226.
(23) Ramachandran, P.; Varoquaux, G. *Mayavi2 User Guide*, 2008.
(24) Koppi, K.; Tirrell, M.; Bates, F. *Phys. Rev. Lett.* **1993**, *70*, 1449−1452.
(25) Koppi, K.; Tirrell, M.; Bates, F.; Almdal, K.; Colby, R. *J. Phys. II* **1992**, *2*, 1941−1959.
(26) Patel, S.; Larson, R.; Winey, K.; Watanabe, H. *Macromolecules* **1995**, *28*, 4313−4318.
(27) Riise, B.; Fredrickson, G.; Larson, R.; Pearson, D. *Macromolecules* **1995**, *28*, 7653−7659.
(28) Gupta, V.; Krishnamoorti, R.; Kornfield, J.; Smith, S. *Macromolecules* **1995**, *28*, 4464−4474.
(29) Leist, H.; Maring, D.; Thurn-Albrecht, T.; Wiesner, U. *J. Chem. Phys.* **1999**, *110*, 8225.
(30) Fredrickson, G. *J. Rheol.* **1994**, *38*, 1045−1068.
(31) Rychkov, I. *Macromol. Theory Simul.* **2005**, *14*, 207−242.
(32) Chen, Z.; Kornfield, J. *Polymer* **1998**, *39*, 4679−4699.
(33) Hamley, I. *Curr. Opin. Colloid Interface Sci.* **2000**, *5*, 341−349.
(34) Guo, H.; Kremer, K.; Soddemann, T. *Phys. Rev. E* **2002**, *66*, 061503.
(35) Guo, H. *J. Chem. Phys.* **2006**, *124*, 054902.
(36) Liu, W.; Qian, H.; Lu, Z.; Li, Z.; Sun, C. *Phys. Rev. E* **2006**, *74*, 021802.
(37) Cui, J.; Ma, Z.; Li, W.; Jiang, W. *Chem. Phys.* **2011**, *386*, 81−87.
(38) Groot, R.; Madden, T.; Tildesley, D. *J. Chem. Phys.* **1999**, *110*, 9739.
(39) Groot, R.; Madden, T. *J. Chem. Phys.* **1998**, *108*, 8713.
(40) Groot, R.; Warren, P. *J. Chem. Phys.* **1997**, *107*, 4423.
(41) Fraser, B.; Denniston, C.; Müser, M. *J. Chem. Phys.* **2006**, *124*, 104902.
(42) Lísal, M.; Brennan, J. *Langmuir* **2007**, *23*, 4809−4818.
(43) Edwards, E.; Stoykovich, M.; Müller, M.; Solak, H.; De Pablo, J.; Nealey, P. *J. Polym. Sci., Part B: Polym. Phys.* **2005**, *43*, 3444−3459.
(44) Edwards, E.; Müller, M.; Stoykovich, M.; Solak, H.; de Pablo, J.; Nealey, P. *Macromolecules* **2007**, *40*, 90−96.
(45) Detcheverry, F.; Liu, G.; Nealey, P.; de Pablo, J. *Macromolecules* **2010**, *43*, 3446−3454.
(46) Pike, D.; Detcheverry, F.; Müller, M.; de Pablo, J. *J. Chem. Phys.* **2009**, *131*, 084903.
(47) Detcheverry, F.; Kang, H.; Daoulas, K.; Müller, M.; Nealey, P.; de Pablo, J. *Macromolecules* **2008**, *41*, 4989−5001.
(48) Detcheverry, F.; Pike, D.; Nagpal, U.; Nealey, P.; Pablo, J. *Soft Matter* **2009**, *5*, 4858−4865.
(49) Nagpal, U.; Detcheverry, F.; Nealey, P.; de Pablo, J. *Macromolecules* **2011**, *44*, 3444−3459.
(50) Detcheverry, F.; Nealey, P.; de Pablo, J. *Macromolecules* **2010**, *43*, 6495−6504.
(51) Liu, G.; Ramírez-Hernández, A.; Yoshida, H.; Nygård, K.; Satapathy, D.; Bunk, O.; de Pablo, J.; Nealey, P. *Phys. Rev. Lett.* **2012**, *108*, 065502.
(52) Liu, G.; Detcheverry, F.; Ramírez-Hernández, A.; Yoshida, H.; Tada, Y.; de Pablo, J.; Nealey, P. *Macromolecules* **2012**, *45*, 3986−3992.
(53) Ramírez-Hernández, A.; Liu, G.; Nealey, P.; de Pablo, J. *Macromolecules* **2012**, *45*, 2588−2596.
(54) Lees, A.; Edwards, S. *J. Phys. C: Solid State Phys.* **1972**, *5*, 1921.
(55) Daoulas, K.; Müller, M.; Pablo, J.; Nealey, P.; Smith, G. *Soft Matter* **2006**, *2*, 573−583.
(56) Ramírez-Hernández, A.; Detcheverry, F.; Peters, B. L.; Chappa, V. C.; Morse, M. C.; Müller, M.; de Pablo, J. J. In preparation.
(57) Pastorino, C.; Kreer, T.; Müller, M.; Binder, K. *Phys. Rev. E* **2007**, *76*, 026706.
(58) Espanol, P.; Warren, P. *Europhys. Lett.* **1995**, *30*, 191.
(59) Hoogerbrugge, P.; Koelman, J. *Europhys. Lett.* **1992**, *19*, 155.
(60) Müller-Plathe, F. *Phys. Rev. E* **1999**, *59*, 4894.
(61) Khandpur, A.; Foerster, S.; Bates, F.; Hamley, I.; Ryan, A.; Bras, W.; Almdal, K.; Mortensen, K. *Macromolecules* **1995**, *28*, 8796−8806.
(62) Varnik, F.; Baschnagel, J.; Binder, K. *J. Chem. Phys.* **2000**, *113*, 4444.
(63) Maniadis, P.; Lookman, T.; Kober, E.; Rasmussen, K. *Phys. Rev. Lett.* **2007**, *99*, 48302.
(64) Doi, M.; Edwards, S. *The Theory of Polymer Dynamics*; Oxford University Press: New York, 1988; Vol. 73.
(65) De Gennes, P. *Scaling Concepts in Polymer Physics*; Cornell University Press: Ithaca, NY, 1979.
(66) Müller, M.; Pastorino, C. *Europhys. Lett.* **2008**, *81*, 28002.
(67) Helfand, E. *Macromolecules* **1975**, *8*, 552−556.
(68) Noguchi, H.; Gompper, G. *Phys. Rev. E* **2008**, *78*, 016706.